Incomplete neutrino decoupling effect on big bang nucleosynthesis

Julien Froustey[1, *] and Cyril Pitrou[1]

[1] *Institut d'Astrophysique de Paris, CNRS UMR 7095, Sorbonne Université, 98 bis Bd Arago, 75014 Paris, France*

(Dated: December 20, 2019)

In the primordial Universe, neutrino decoupling occurs only slightly before electrons-positrons annihilations, leading to an increased neutrino energy density with order 10^{-2} spectral distortions compared to the standard instantaneous decoupling approximation. However, there are discrepancies in literature on the impact it has on the subsequent primordial nucleosynthesis, not only on the magnitude of the abundance modifications, but also on their sign. We review how neutrino decoupling affects indirectly the various stages of nucleosynthesis, namely the freezing out of neutron abundance, the duration of neutron beta decay, and the nucleosynthesis itself. This allows to predict the sign of abundance variations which are expected when the physics of neutrino decoupling is taken into account. For simplicity, we ignore neutrino oscillations, but we conjecture from the detailed interplay of neutrino temperature shifts and distortions that their effect on final light elements abundances should be subdominant.

I. INTRODUCTION

The production of light elements during the first few minutes of our Universe, known as big bang nucleosynthesis (BBN), is a robust prediction of the standard cosmological model. The observational constraints on ^{4}He [1, 2] and deuterium abundances [3–5] have now reached a percent level precision, and the baryon abundance, which is the only free cosmological parameter which controls the synthesis, is also measured with a percent precision from cosmic microwave background (CMB) anisotropies [6]. In order to use BBN to constrain exotic cosmologies, or even to check the consistency of the theory with the one inferred from large scale structure and CMB, it has thus become crucial to develop a theory of BBN which is much more precise than its associated observational constraints. Hence, we aim at least at a 10^{-3} precision level in the theory, and ideally even 10^{-4}. The ^{4}He abundance is essentially set by the neutron-to-proton ratio, which is in turn controlled by weak interaction rates. A comprehensive list of small physical effects, including radiative corrections, has been developed in Refs. [7–11], and reviewed in Ref. [12], so as to reach a 0.1 % theoretical precision on the weak rates. Numerical codes such as `PArthENoPE` [13, 14], `AlterBBN` [15, 16] and `PRIMAT` [12], developed to predict these abundances, now incorporate these small physical effects, though with different approximations. The final abundances of other light elements, which are only at the level of traces, depend also directly on nuclear reaction rates, which themselves are also only known with a few percent precision in general, and can also be subject to radiative corrections [17].

Among the small effects which affect these abundances is the incomplete decoupling of neutrinos prior to the reheating of photons by electrons-positrons annihilations when the temperature of the Universe drops below 1 MeV. It leads to a small modification of the energy density in neutrinos [18–21], affecting the Hubble expansion rate. Therefore a full treatment of the decoupling physics is required to describe properly the outcome of BBN. In this paper, we improve `PRIMAT`'s predictions by considering the detailed effects of incomplete neutrino decoupling. We choose to leave aside the effect of neutrino oscillations, and focus instead on the effect of decoupling alone, as this will allow a physical understanding of how it influences final abundances. We comment further that from the understanding of the physics at play, it is expected that neutrino oscillations preserve the essential effects of neutrino decoupling, even though they alter the neutrino spectral distortions.

As far as we are aware, there are currently three references which have studied the effect of decoupling on BBN abundances beyond the ^{4}He prediction, but they reach different conclusions as for the sign of abundance modifications. In Table 3 of Ref. [20], it is found that ^{4}He and ^{7}Li abundances are increased, whereas deuterium and ^{3}He abundances are decreased, due to incomplete decoupling of neutrinos. However, in Ref. [21], but also in Ref. [12], it is found that the variations are exactly in opposite directions for all these abundances but ^{4}He. This is all the more surprising since Ref. [12] does not solve independently for the neutrino decoupling, but uses the neutrino heating function of Ref. [13]. It should nevertheless be noted that the abundances of other elements than ^{4}He were not the main focus of Ref. [20], since precise measurements of deuterium abundance were not available at that time.

The goal of this paper is to gain insight in the physics of neutrino decoupling on BBN, so as to understand in which sense, and to what extent, the abundances are affected. To that purpose, we have developed an independent implementation of the neutrino decoupling dynamical equations (without flavor oscillations), whose main ingredients and results for the neutrino spectra modifications are gathered in the next section, along with technical details in appendix. In section III, we then review how

* froustey@iap.fr

final BBN abundances are modified by coupling these results to `PRIMAT`.

Comparisons with respect to a fiducial cosmology, where neutrino are artificially decoupled instantaneously prior to electrons-positrons annihilations, require to be able to map different homogeneous cosmologies. There is no unique way to perform this cosmology mapping, that is to compute variations, exactly like there is a gauge freedom when comparing a perturbed cosmology with a background cosmology. For instance, we can compare the fiducial instantaneous decoupling with the full neutrino decoupling physics, either using the same cosmological times, or the same cosmological factors, or even the same plasma temperatures. The fact that there is no unique choice complicates the discussion of the physical effects at play, but the physical observables, e.g. the final BBN abundances, do not depend on it. We will systematically specify which variable is left constant (cosmic time, scale factor, or photon temperature) when comparing the true Universe to the fiducial one. Quantities written with a superscript $^{(0)}$ correspond to the fiducial (instantaneous decoupling) cosmology, and the variation of a quantity ψ will be written

$$\delta\psi \equiv \frac{\Delta\psi}{\psi^{(0)}} \equiv \frac{\psi - \psi^{(0)}}{\psi^{(0)}} \,. \tag{1}$$

II. NEUTRINO DECOUPLING

A. Neutrino kinetic equations

The evolution of neutrino distribution functions is described by the Boltzmann equation

$$\left[\frac{\partial}{\partial t} - Hp\frac{\partial}{\partial p}\right] f_{\nu_\alpha}(p,t) = C_{\nu_\alpha}[f_\nu, f_{e^\pm}] \,, \tag{2}$$

where $C_{\nu_\alpha}[f_j]$ is the collision term. This collision integral is dominated by two-body reactions such as the annihilation process $\nu_\alpha + \bar{\nu}_\alpha \leftrightarrow e^- + e^+$ or neutrino-charged lepton scattering $\nu_\alpha + e^\pm \leftrightarrow e^\pm + \nu_\alpha$. The matrix elements for all relevant weak interaction processes are collected in e.g. Ref. [21] (see also Refs. [18, 22]).

We consider the case without neutrino asymmetry for which $f_{\nu_\alpha} = f_{\bar{\nu}_\alpha}$. We also assume that the distribution functions are the same for ν_μ and ν_τ, since at the energy scales of interest, typically the MeV, the muon and tau neutrinos have the same interactions with electrons and positrons. This is not true for electron neutrinos which interact with the background $e^\pm$ via charged-current processes in addition to neutral-current channels. The set of equations is conveniently rewritten for numerical implementation in terms of comoving variables [20, 23]:

- the normalized scale factor $x \equiv m_e/T_{\rm cm}$ (used in practice as an integration variable);
- the comoving momentum $y \equiv p/T_{\rm cm}$;
- the dimensionless photon temperature $z \equiv T_\gamma/T_{\rm cm}$;

where the comoving temperature $T_{\rm cm} \propto a^{-1}$ is only a convenient proxy for the scale factor [21], and does not necessarily correspond to a physical temperature except at high values $T_{\rm cm} \gg 1$ MeV where all species are strongly coupled, hence $T_\nu = T_\gamma = T_{\rm cm}$.

In the instantaneous decoupling approximation, neutrinos have an equilibrium Fermi-Dirac (FD) distribution at temperature $T_{\rm cm}$, which reads

$$f_\nu^{(0)}(y) \equiv \frac{1}{e^y + 1} \,. \tag{3}$$

The charged leptons (electrons and positrons) are, in the range of temperatures of interest, kept in equilibrium with the plasma by fast electromagnetic interactions [24]. Therefore they follow a Fermi-Dirac distribution[1] at the plasma temperature T_γ, written as

$$f_{e^\pm} = \frac{1}{e^{\sqrt{p^2+m_e^2}/T_\gamma} + 1} = \frac{1}{e^{\sqrt{y^2+x^2}/z} + 1} \,. \tag{4}$$

We need to solve for the evolution of the neutrino distribution functions and the photon temperature, i.e. the three variables $f_{\nu_e}(x,y)$, $f_{\nu_\mu}(x,y)$ and $z(x)$. In addition to the Boltzmann equations for neutrinos (2), rewritten in the form

$$\frac{\partial f_{\nu_\alpha}(x,y)}{\partial x} = \frac{1}{xH} C_{\nu_\alpha}(x,y) \,, \tag{5}$$

the third dynamical equation is the homogeneous energy conservation equation $\dot{\rho} = -3H(\rho + P)$. Following Ref. [23], it proves convenient for the stability of numerical implementations to introduce the dimensionless thermodynamic quantities

$$\bar{\rho} \equiv \rho \left(\frac{x}{m_e}\right)^4 , \qquad \bar{P} \equiv P \left(\frac{x}{m_e}\right)^4 . \tag{6}$$

The energy conservation equation is then recast as an equation for $z(x)$ [19, 23].

A comprehensive treatment of neutrino decoupling also requires to take into account two other effects. First, the electromagnetic interactions in the thermal bath of electrons, positrons and photons lead to corrections with respect to vacuum quantum field theory. The plasma thermodynamics are modified through a change of the dispersion relations of $e^\pm$ and photons [9, 25, 26], which up to order e^2 can be described as a mass shift [27]. These QED corrections to the energy density and the pressure lead to corrective terms in the equation on $z(x)$, whose expressions are given in Mangano *et al.* [19]. In addition,

[1] The electrons/positrons dimensionless chemical potential μ_e/T_γ can be safely neglected as it is of order of the baryon to photon ratio during most of the time of interest, that is smaller than 10^{-9}, see e.g. Fig. 30 in Ref. [12].

they claim that the modified dispersion relations must be introduced in the $f_{e^\pm}$ distribution functions, thus modifying the rates. However, and as pointed out in Ref. [12] for neutron/proton weak reactions, the mass shift is just part of the full finite-temperature radiative corrections for the weak rates derived in Ref. [10]. A comprehensive study of the finite-temperature corrections to neutrino weak rates is thus still needed, and we only input QED corrections in the plasma thermodynamics[2].

The second effect which needs to be taken into account is neutrino flavor oscillations, and it requires to trade distribution functions for a density matrix formalism [28, 29]. The computation of collision integrals is considerably more demanding, and this has been progressively done in the last decade [20, 30]. Nevertheless, understanding the physical phenomena involved in the effect of incomplete neutrino decoupling on primordial nucleosynthesis, even without oscillations, will serve as a guideline to forecast the effect of oscillations, based on the variation of a small number of quantities introduced in the following.

Throughout this paper, we will never consider neutrino oscillations, and QED corrections will not be included unless specified.

B. Numerical implementation

Two options have been considered to solve the kinetic equations. Either we use a discretization in momentum [18, 21], the only method to have a reasonable computation time, or we expand the distribution functions in a basis of polynomials [23], so as to avoid extrapolation of distribution functions between binning points. To combine both advantages, we use a hybrid method with both orthonormal polynomials and a discretization in momentum. The neutrino distribution function is separated into an FD equilibrium one and a distortion according to

$$f_{\nu_\alpha}(x,y) = \frac{1}{e^y+1}\left[1+\delta f_{\nu_\alpha}(x,y)\right] . \tag{7}$$

We then expand δf_{ν_α} in a set of polynomials

$$\delta f_{\nu_\alpha}(x,y) = \sum_{i=0}^{\infty} a_i^\alpha(x) P_i(y) \simeq \sum_{i=0}^{3} a_i^\alpha(x) P_i(y) , \tag{8}$$

where the polynomials P_i are orthonormal with respect to the FD weight,

$$\int_0^\infty \mathrm{d}y \frac{1}{e^y+1} P_i(y) P_j(y) = \delta_{ij} . \tag{9}$$

[2] For completeness, we checked what happens if we include the mass shifts in the distribution functions, following Ref. [19]. The results are identical at the level of precision considered, which is not surprising since computing collision integrals without the mass shift is already a first order correction compared to the instantaneous decoupling case where collision integrals vanish by definition.

The numerical results indicate, in agreement with Refs. [19, 23], that going up to order 3 polynomials is sufficient for our level of precision. Using the expansion (8), the Boltzmann equation (5) becomes

$$\frac{da_i^\alpha(x)}{dx} = \frac{1}{xH}\int_0^\infty \mathrm{d}y_1\, P_i(y_1)\, C_{\nu_\alpha}(x,y_1) . \tag{10}$$

The explicit expression of C_{ν_α} and the differential equation for $z(x)$ are collected in the Appendix A.

The initial time of integration results from a compromise, as it must be early enough to capture all the relevant features of decoupling, but late enough such that weak rates are not too large, which would result in numerical stiffness when evaluating the collision integrals. We follow Refs. [18, 23] and take an initial (comoving) temperature $T_{\rm cm}^{\rm (in)} = 10$ MeV, which corresponds to $x_{\rm in} = 0.0511$.

Neutrinos are kept in thermal equilibrium with the electromagnetic plasma before $x_{\rm in}$, so they have initially a FD distribution at the photon temperature, that is

$$f_\nu^{\rm (in)}(y) = \frac{1}{e^{p/T_\gamma^{\rm (in)}}+1} = \frac{1}{e^{y/z_{\rm in}}+1} , \tag{11}$$

which determines the initial values of the coefficients a_i^α. Note that since electrons and positrons are not fully relativistic at $T_{\rm cm}^{\rm (in)}$, $z_{\rm in}$ is not exactly 1. Writing entropy conservation of the full system of electrons, positrons, neutrinos, antineutrinos and photons, one infers $z_{\rm in} = 1.00003$, as in Ref. [31]. Besides, we checked that QED corrections to the plasma thermodynamics do not change $z_{\rm in}$ at this level of precision.

In agreement with previous statements in the literature [18, 20, 21], we find that a binning in momentum y with at least 100 points in the range $[0, 20]$ is sufficient to ensure convergence. Specifically, we chose a grid of 150 equally spaced points between $y_{\rm min} = 0.1$ and $y_{\rm max} = 20$. As for the integration variable x, it ranges from $x_{\rm in} = 0.0511$ to $x_{\rm fin} \simeq 60$ where decoupling is essentially over.

C. Results for neutrino transport

1. *Overview*

The final dimensionless photon temperature is $z_{\rm fin} \simeq 1.3991$ (without QED corrections), which must be contrasted to the instantaneous decoupling value $z_0 = (11/4)^{1/3} \simeq 1.40102$. As expected, e^+e^- annihilations partly heat the neutrinos and the electromagnetic plasma is consequently less reheated. Including QED corrections, we get $z_{\rm fin} \simeq 1.3979$. These values are in very good agreement with previous results[3] [21, 30].

[3] Grohs *et al.* [21] obtain a lower value for $z_{\rm fin}$ when including QED corrections, but this is due to an incorrect "non-perturbative" implementation, as pointed out in Refs. [12, 27]. It is corrected in Ref. [32].

The distortions with respect to the equilibrium Fermi-Dirac distribution are displayed on Fig. 1, where we plot δf_ν – as defined in Eq. (7) – for comoving momenta $y = 3$, 5 and 7. Due to the contribution of charged-current processes, ν_e distortions are enhanced with respect to the ones for ν_μ and ν_τ, and the associated freeze-out occurs later. Note that neutrino distortions are of order $\delta f_\nu \sim 10^{-2}$, which is considerably larger than CMB spectral distortions [33].

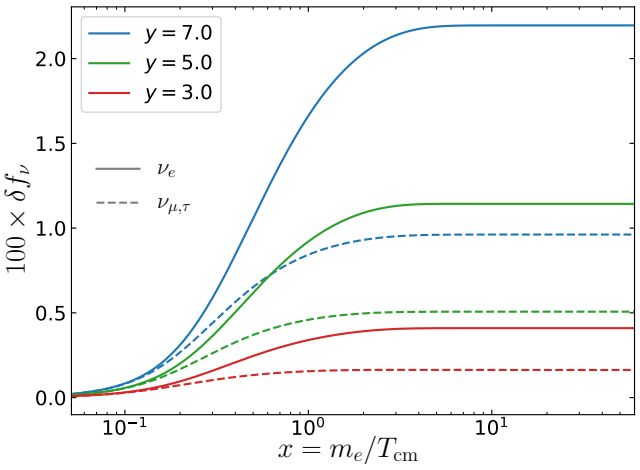

FIG. 1. Evolution of the distortion δf_ν as a function of x. From bottom to top: $y = 3$, $y = 5$ and $y = 7$. Solid (resp. dashed) lines correspond to electron (resp. muon/tau) neutrinos. It shows agreement with Fig. 1 in Ref. [21], Fig. 3 in Ref. [18] and Fig. 4 in Ref. [23].

.

Accordingly, we observe an increase of the energy density of neutrinos

$$\delta\rho_{\nu_\alpha} \equiv \frac{\rho_{\nu_\alpha} - \rho^{(0)}_{\nu_\alpha}}{\rho^{(0)}_{\nu_\alpha}}\,, \tag{12}$$

with asymptotic values $\delta\rho_{\nu_e} \simeq 0.93\,\%$ and $\delta\rho_{\nu_{\mu,\tau}} \simeq 0.39\,\%$ (since these are frozen-out values, it is equivalent to compute them at constant x or T_γ), still in excellent agreement with previous results. Through Friedmann equation, the expansion rate of the Universe is consequently modified, which has important consequences on primordial nucleosynthesis.

2. *Effective description of neutrinos*

To scrutinize the precise role of neutrinos in BBN, it is particularly important to use a parametrization which separates the different effects of incomplete decoupling. To this end, we define an effective neutrino temperature T_ν (there is no genuine temperature since the distribution is not at equilibrium) as the temperature of the FD distribution with zero chemical potential which would have the same energy density as the real distribution, that is

$$\rho_{\nu_\alpha} \equiv \frac{7}{8}\frac{\pi^2}{30}T^4_{\nu_\alpha} \iff \bar\rho_{\nu_\alpha} \equiv \frac{7}{8}\frac{\pi^2}{30}z^4_{\nu_\alpha}\,. \tag{13}$$

Distortions are then defined with respect to this FD spectrum, according to

$$f_{\nu_\alpha}(x,y) = \frac{1}{e^{y/z_{\nu_\alpha}(x)}+1}\left[1+\delta g_{\nu_\alpha}(x,y)\right]\,. \tag{14}$$

By definition, these effective distortions are constrained so that Eq. (13) holds, hence[4]

$$\int_0^\infty {\rm d}y\, y^3 \frac{\delta g_{\nu_\alpha}(y)}{e^{y/z_{\nu_\alpha}}+1} = 0\,. \tag{15}$$

We plot the final effective distortions $\delta g_{\nu_\alpha}(x_{\rm fin} \simeq 60, y)$ as a function of momentum on Fig. 2. Even though these distortions and δf_{ν_α} (shown in Fig. 2 of Ref. [21]) are defined with respect to different references, their overall shapes are similar. This is expected since $z_{\nu_\alpha} \simeq 1$, and compared to a purely thermal distribution there is a deficit of low-energy neutrinos because of interactions with the hotter electrons and positrons, hence the negative values of δg_{ν_α} for $y \leq 5$.

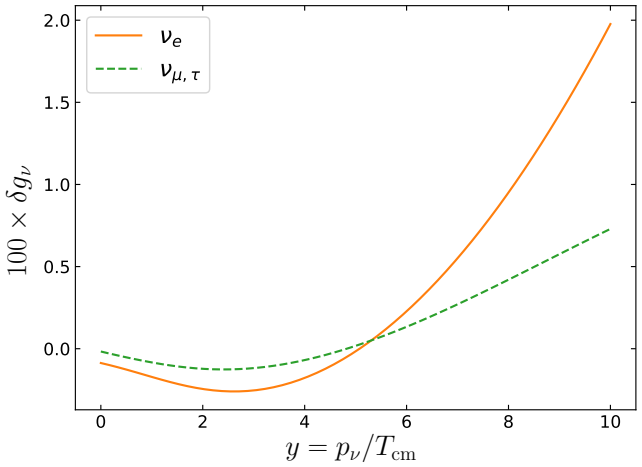

FIG. 2. Distortions with respect to the effective FD spectrum, as defined in Eq. (14). Solid line: electron neutrinos. Dashed line: muon/tau neutrinos.

The final values we obtain are $z^{\rm fin}_{\nu_e} \simeq 1.0023$ and $z^{\rm fin}_{\nu_{\mu,\tau}} \simeq 1.0010$, showing once more the higher reheating

[4] This approach for defining distortions is different from the CMB spectral distortions which are computed numerically using a number density effective temperature, rather than an energy density effective temperature [33]. In the neutrino case, and given the size of distortions which are much larger than for CMB, the neutrino energy density is more adapted since it enters directly in the Friedmann equation governing the expansion rate.

of electron neutrinos. The total neutrino energy density is, taking into account neutrinos and antineutrinos,

$$\bar{\rho}_\nu = 2 \times \frac{7}{8}\frac{\pi^2}{30} \times \left(z_{\nu_e}^4 + 2 z_{\nu_\mu}^4\right) \equiv 3 \times \frac{7}{8}\frac{\pi^2}{15} \times \hat{z}_\nu^4 \,, \quad (16)$$

where we introduced the average effective temperature of neutrinos

$$\hat{z}_\nu \equiv \left(z_{\nu_e}^4 + 2\, z_{\nu_\mu}^4\right)^{\frac{1}{4}} \iff \widehat{T}_\nu \equiv \left(T_{\nu_e}^4 + 2\, T_{\nu_\mu}^4\right)^{\frac{1}{4}} \,. \quad (17)$$

These effective temperatures, being based on energy density, are adapted to the computation of the Hubble expansion rate, since in the very early universe it is determined by the total radiation energy density $\rho_{\rm rad} = \rho_\gamma + \rho_{e^\pm} + \rho_\nu$. In the instantaneous decoupling approximation, we simply have

$$\rho_{\rm rad}^{(0)}(T_{\rm cm}) = \left[1 + \frac{7}{8}\left(\frac{T_{\rm cm}}{T_\gamma^{(0)}}\right)^4 3\right] \rho_\gamma^{(0)} + \rho_{e^\pm}^{(0)} \,, \quad (18)$$

since $\rho_\gamma = (\pi^2/15) T_\gamma^4$. The departure from this standard picture has historically been parametrized through $N_{\rm eff}$, the *effective number of neutrino species*, i.e. the number of instantaneously decoupled neutrino species that would give the same energy density:

$$\rho_\nu(T_{\rm cm}) = \frac{7}{8}\left(\frac{T_{\rm cm}}{T_\gamma^{(0)}}\right)^4 N_{\rm eff} \times \rho_\gamma \,, \quad (19)$$

where $T_\gamma^{(0)}(T_{\rm cm})$ is the photon temperature at a given scale factor in the instantaneous decoupling approximation. Note that we could also define those quantities as a function of T_γ:

$$\rho_\nu(T_\gamma) = \frac{7}{8}\left(\frac{T_{\rm cm}^{(0)}}{T_\gamma}\right)^4 N_{\rm eff} \times \rho_\gamma \,. \quad (20)$$

$N_{\rm eff}$ can either way be expressed as

$$N_{\rm eff} = 3\left(\frac{\hat{z}_\nu z^{(0)}}{z}\right)^4 \,. \quad (21)$$

The final values of all these parameters are summarized in Table I, with comparison to previous results.

With this numerical simulation, we are able to grasp the variety of processes in place during the MeV age, summarized in Fig. 3, where quantities are plotted with respect to a physical quantity, the plasma temperature. The reheating of the different species is due to the entropy transfer from electrons and positrons, which is visualized by plotting the variation of their number density. For $T_\gamma \gg m_e$, electrons are relativistic and $\bar{n}_{e^\pm} \equiv (n_{e^-} + n_{e^+}) \times (x/m_e)^3$ is constant ; while for $T_\gamma \ll m_e$ the density drops to zero. The variation between those two constants corresponds to the annihilation period, which indeed starts around $T_\gamma \sim m_e$ and is over for $T_\gamma \sim 30\,$keV. At the beginning of this period, neutrinos are progressively decoupling and there is a heat transfer from the plasma, visualized through the

Frozen values	z	z_{ν_e}	z_{ν_μ}	$N_{\rm eff}$
No QED corrections				
Instantaneous decoupling	1.40102	1.	1.	3.000
Naples group [20]	1.3990	1.0024	1.0011	3.035
Grohs *et al.* [21]	1.3990	1.0023	1.0009	3.034
This paper	**1.3991**	**1.0023**	**1.0010**	**3.034**
With QED corrections				
Instantaneous decoupling	1.39979	1.	1.	3.011
Naples group [30]	1.39784	1.0023	1.0010	3.045
Grohs *et al.* [32]	1.39782			3.044
This paper	1.39791	1.0023	1.0010	3.044

TABLE I. Comparison of neutrino transport results with previous studies. We have converted energy density increases in effective neutrino temperatures via $\delta\rho_{\nu_\alpha} = z_{\nu_\alpha}^4 - 1$. For QED corrections, we took the most recent values from the Naples group [30] and Grohs *et al.* ([32] instead of [21], where they incorrectly implemented these corrections).

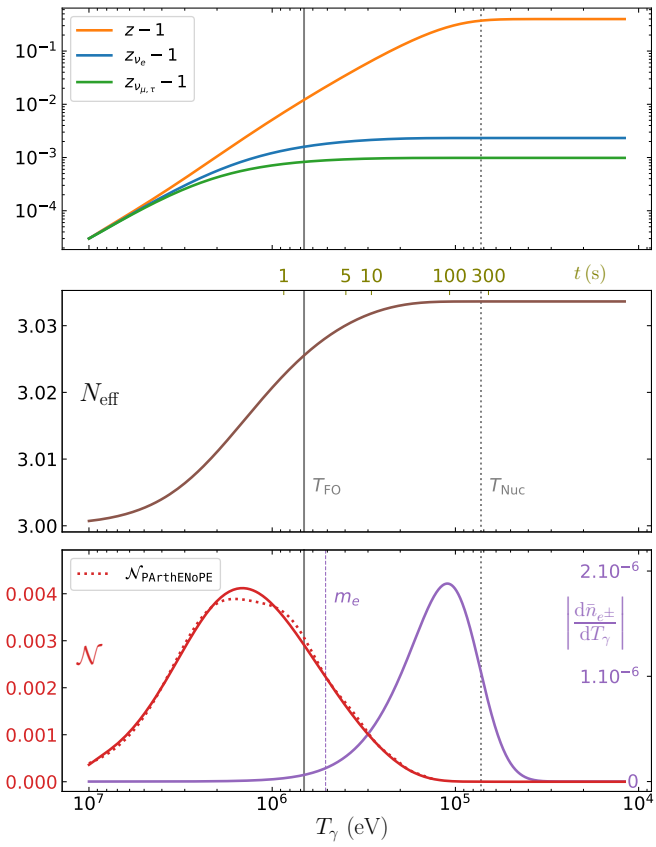

FIG. 3. Evolution of relevant quantities for neutrino decoupling, as a function of the plasma temperature. Top: comoving (effective) temperatures of the plasma and neutrinos. Middle: effective number of neutrinos, as defined in Eq. (21). Bottom: neutrino heating rate and variation of the comoving electron+positron density.

dimensionless heating rate [12–14]

$$\mathcal{N}(z) = \frac{1}{z^4}\left(x\frac{d\bar{\rho}_\nu}{dx}\right)_{x=x(z)} = \frac{1}{z^4}\frac{1}{\pi^2 H}\int_0^\infty \mathrm{d}y\, y^3\left[C_{\nu_e} + 2C_{\nu_\mu}\right]. \quad (22)$$

It is non-zero precisely during the decoupling of neutrinos. The slight overlap between the two curves on the bottom of Fig. 3 is the very reason why neutrinos are partly reheated. Finally we plotted the evolution of $N_{\rm eff}$, from 3 before the MeV age to its frozen value 3.034 (without QED corrections). Comparing with Fig. 5 in Ref. [21], one would note that there is no "plateau" before the freeze-out. This behaviour can be considered as an artifact due to plotting $N_{\rm eff}$ as a function of $x = m_e/T_{\rm cm}$: the plateau is due to the difference $T_{\rm cm}/T_{\rm cm}^{(0)}$ for a given T_γ, and does not represent a meaningful physical effect.

III. CONSEQUENCES ON BIG BANG NUCLEOSYNTHESIS

By modifying the expansion rate of the Universe and affecting the neutron/proton weak reaction rates, incomplete neutrino decoupling will slightly modify the BBN abundances of light elements [12, 20, 21]. We incorporate the results of Section II in the BBN code `PRIMAT` to investigate the associated modification of abundances.

If n_i is the volume density of isotope i, and n_b the baryon density, we define $Y_i \equiv n_i/n_b$ the *number* fraction of isotope i. The *mass* fraction is therefore $X_i \equiv A_i Y_i$, with A_i the nucleon number. It is customary to define $Y_{\rm P} \equiv X_{^4\rm He}$ and $i/{\rm H} \equiv Y_i/Y_{\rm H}$.

To get a clear understanding of the physics at play, it is useful to recall the standard picture of BBN [34].

1. Neutrons and protons track their equilibrium abundances

$$\left.\frac{n_n}{n_p}\right|_{\rm eq} = \exp\left(-\Delta/T_\gamma\right),$$

with $\Delta = m_n - m_p \simeq 1.293\,{\rm MeV}$ the difference of nucleon masses, until the so-called "weak freeze-out", when the rates of $n \leftrightarrow p$ reactions drop below the expansion rate,

$$\gamma \equiv \left.\frac{\Gamma_{n\to p} + \Gamma_{p\to n}}{H}\right|_{T_{\rm FO}} \simeq 1. \quad (23)$$

2. After the freeze-out, neutrons only undergo beta decay until the beginning of nucleosynthesis, and a good approximation is

$$X_n(T_{\rm Nuc}) = X_n(T_{\rm FO}) \times \exp\left[-\frac{t_{\rm Nuc} - t_{\rm FO}}{\tau_n}\right], \quad (24)$$

where $\tau_n \simeq 879.5\,{\rm s}$ is the neutron mean lifetime. The nucleosynthesis temperature is usually defined when the *deuterium bottleneck* is overcome, with the criterion $n_D/n_b \sim 1$ [34, 35]. It can also be associated to the maximum in deuterium abundance [36] which coincides with the drop in the density of neutrons, converted into heavier elements. We will adopt this definition, which is anyway very close to the other criterion. Note that $t_{\rm Nuc} - t_{\rm FO} \simeq t_{\rm Nuc}$ since $t_{\rm FO} \ll t_{\rm Nuc}$.

3. Almost all free neutrons are then converted in ^{4}He, leading to

$$Y_{\rm P} \simeq 2X_n(T_{\rm Nuc}). \quad (25)$$

This indicates where neutrinos incomplete decoupling will intervene. Weak rates, and thus the freeze-out temperature, are modified through the changes of distribution functions (different temperatures and spectral distortions δg_{ν_e}). But the changes in energy density will also modify the relation $t(T_\gamma)$, leaving more or less time for neutron beta decay and light elements production. This is the so-called *clock effect* originally discussed in Refs. [37, 38]. In summary, the neutron fraction at the onset of nucleosynthesis is modified as

$$\delta X_n^{[\rm Nuc]} = \frac{\Delta X_n(T_{\rm Nuc})}{X_n^{(0)}(T_{\rm Nuc})} = \frac{\Delta X_n(T_{\rm FO})}{X_n^{(0)}(T_{\rm FO})} - \frac{\Delta t_{\rm Nuc}}{\tau_n}, \equiv \delta X_n^{[\rm FO]} + \delta X_n^{[\Delta t]}, \quad (26)$$

with $\Delta t_{\rm Nuc} \equiv t_{\rm Nuc} - t_{\rm Nuc}^{(0)}$ (we neglected the variation of $t_{\rm FO}$). For freeze-out ($\delta X_n^{[\rm FO]}$), it is a variation at constant $\gamma = 1$, taken as our definition of freeze-out. $\delta X_n^{[\rm Nuc]}$ is the neutron abundance variation between the onset of nucleosynthesis in the "actual" Universe and the one in the reference Universe. Given our definition of $T_{\rm Nuc}$, the constant quantity is here $\mathrm{d}X_D/\mathrm{d}t = 0$.

A. Incomplete neutrino decoupling in `PRIMAT`

In the version of `PRIMAT` used in Ref. [12], the lack of effective temperatures and spectral distortions values across the nucleosynthesis era required an approximate strategy to include incomplete neutrino decoupling. It consisted in neglecting spectral distortions $\delta g_\nu = 0$, but computing an effective average temperature $\widehat{T}_\nu$ from the heating rate (22). The values of $\mathcal{N}$ were obtained from a fit given in `PArthENoPE` [13] [Eqs. (A23)–(A25)], computed by Pisanti *et al.* from the results of Refs. [19, 20].

This method captures correctly the changes in the expansion rate (since the energy density is well computed from $\widehat{T}_\nu$), but it handles *a priori* badly the weak rates: electron neutrinos are too cold ($T_{\nu_e} > \widehat{T}_\nu$), and their spectrum is not distorted. This should in principle have consequences on the neutron-to-proton ratio at freeze-out, thus on final abundances.

We modified `PRIMAT` to introduce the results from neutrino transport analysis. Since the useful variable in

BBN framework	$Y_{\rm P}$	$\delta Y_{\rm P}$ (%)	D/H $\times 10^5$	δ(D/H) (%)	$\left({}^3{\rm He}+{\rm T}\right)/{\rm H}\times 10^5$	$\left({}^7{\rm Li}+{}^7{\rm Be}\right)/{\rm H}\times 10^{10}$
Inst. decoupling, no QED	0.24262	0	2.423	0	1.069	5.635
$\widehat{T}_\nu$	0.24274	0.050	2.433	0.38	1.070	5.613
T_{ν_e}, no distortions	0.24266	0.015	2.432	0.36	1.070	5.612
T_{ν_e}, with distortions	0.24276	0.056	2.433	0.39	1.070	5.613
Inst. decoupling, with QED	0.24262	0	2.426	0	1.069	5.627
$\widehat{T}_\nu$	0.24274	0.050	2.435	0.38	1.070	5.606
T_{ν_e}, no distortions	0.24265	0.015	2.435	0.36	1.070	5.604
T_{ν_e}, with distortions	0.24275	0.056	2.435	0.38	1.070	5.606

TABLE II. Light elements abundances, at the Born approximation level, for various implementations of neutrino-induced corrections. See Section III C for results with the full corrections derived in [12]. Since tritium and ^{7}Be decay respectively into ^{3}He and ^{7}Li, their abundances are usually summed.

nucleosynthesis is the plasma temperature T_γ, all other quantities (x, T_{ν_α}, a_i^α) are interpolated. Depending on options chosen, one can then use the "real" effective neutrino temperatures, or the average one for comparison with the previous approach (keeping in each case the true total energy density). The distortions δg_{ν_e} are computed thanks to the coefficients a_i^e, and correct the weak rates at the Born level. Following the notations of Ref. [12] (Eq. (76) and subsequent), we add the corrections

$$\Delta\Gamma_{n\to p} = K\int_0^\infty p^2{\rm d}p\left[\delta\chi_+(E)+\delta\chi_+(-E)\right], \quad (27a)$$

$$\Delta\Gamma_{p\to n} = K\int_0^\infty p^2{\rm d}p\left[\delta\chi_-(E)+\delta\chi_-(-E)\right], \quad (27b)$$

with $K=\left(m_e^5\lambda_0\tau_n\right)^{-1}$, $E=\sqrt{p^2+m_e^2}$ the electron energy and

$$\delta\chi_\pm(E) = \left(E_\nu^\mp\right)^2 f_e(-E)\frac{{\rm sgn}\left(E_\nu^\mp\right)\times\delta g_{\nu_e}(|E_\nu^\mp|)}{e^{|E_\nu^\mp|/T_{\nu_e}}+1}, \quad (28)$$

$$E_\nu^\mp = E\mp\Delta\,. \quad (29)$$

The sgn function accounts for the fact that $f_{\nu_e}(|E_\nu^\mp|)$ appears as part of a Pauli blocking factor if $E_\nu^\mp<0$, i.e. the neutrino is in a final state.

Our results are summarized in Table II. We considered three different implementations:

- *(i)* the earlier `PRIMAT` approach (no distortions and an average neutrino temperature), with slight differences compared to Ref. [12] since our results are used instead of `PArthENoPE`'s ones;
- *(ii)* input the real electron neutrino temperature in weak rates, but still without spectral distortions;
- *(iii)* full results from neutrino evolution.

Note that these three scenarios take place in identical cosmologies, with the *same* energy density ; using the proper ν_e temperature and including distortions only affect the weak rates. This emphasizes the particular role of spectral distortions: the most striking – and somehow unexpected – feature is the proximity of results in the cases *(i)* and *(iii)*, which is further investigated in the next section.

The results from previous implementations of incomplete neutrino decoupling in BBN codes are shown in Table III, and we check that our results are in close agreement with Grohs *et al.* [21], but with opposite signs of variation (except for ^{4}He) compared to the ones by Mangano *et al.* [20]. The extensive study in the next section sheds a new light on the different phenomena involved.

B. Detailed analysis

We now review the physics which allows to understand the numerical results of Table II. We shall first detail the physics affecting helium abundance, which is directly related to the neutron fraction at the onset of nucleosynthesis, before turning to the other light elements production, for which the clock effect dominates.

1. *Neutron/proton freeze-out*

Previous articles [20, 37, 38] studied the variation of $n\leftrightarrow p$ rates due to incomplete neutrino decoupling at constant scale factor, claiming that H was left unchanged at a given x. This argument of constant total energy density, namely $\Delta\rho_\nu=-\Delta\rho_{\rm em}$, requires $T_\gamma\simeq T_\nu$ (cf. Appendix 3 in Ref. [37]). However by looking at Fig. 3, top panel, it appears that at freeze-out T_γ and T_{ν_α} differ by $\sim 1\,\%$, which is the typical order of magnitude of variations we are interested in. Moreover, the analysis of Ref. [37] uses thermal-equivalent distortions of neutrinos spectra (i.e. only effective temperatures, no δg_ν) and the numerical relation $\Delta X_n^{\rm [FO]}\simeq -0.1\Delta T_i/T_i$, which requires to separate the temperature variations of the different species, seemingly inconsistently with the constant

Variation of abundances	$\delta Y_{\rm P}$	$\delta\,({\rm D/H})$	$\delta\left(({}^3{\rm He}+{\rm T})/{\rm H}\right)$	$\delta\left(({}^7{\rm Li}+{}^7{\rm Be})/{\rm H}\right)$
No QED corrections				
Naples group [20]	6.06×10^{-4}			
Grohs *et al.* [21]	4.636×10^{-4}	3.686×10^{-3}	1.209×10^{-3}	-3.916×10^{-3}
This paper	5.636×10^{-4}	3.869×10^{-3}	1.268×10^{-3}	-3.867×10^{-3}
QED corrections included				
Naples group [20]	6.96×10^{-4}	-2.8×10^{-3}	-1.0×10^{-3}	3.77×10^{-3}
This paper	5.604×10^{-4}	3.831×10^{-3}	1.256×10^{-3}	-3.828×10^{-3}

TABLE III. Comparison with previous results. Note that baseline values are different in the cases including or not QED corrections, see Table II. The values given by the Naples group in Ref. [20] are absolute variations, and we need the baseline values to compute relative variations. These not being given, we used our own baseline values.

energy density requirement. Their results are nonetheless in good agreement with numerical results ; yet our findings seem to indicate that the proper way to implement thermal-equivalent distortions is with a unique, average neutrino temperature, thus modifying slightly the arguments in Refs. [20, 38].

Due to the rich interplay of processes involved, an analytical estimate of $\delta X_n^{\rm [FO]}$ is particularly challenging. Since our goal is to provide a satisfying physical picture of the role of neutrinos in BBN, and thus to check Eq. (26), we used a numerical evaluation. Fig. 4 shows the variation of X_n and $T_{\nu_e,\gamma}$ for the different implementations of neutrino-induced corrections around the time of freeze-out. In each case, incomplete neutrino decoupling leads to a decrease of X_n. We also find the interesting feature, already evidenced in Table II, that a thermal-equivalent approach (without distortions) with an average neutrino temperature gives close results to the full description.

For each implementation of neutrino-induced corrections, the evolution of the photon temperature $z(x)$ is the same, the difference lying in including or not z_{ν_e} and δg_{ν_e}. But the quantities on Fig. 4 are plotted with respect to γ, which is a different function of x in each case. For instance when including the real ν_e temperature, weak rates increase and freeze-out is delayed, hence a smaller $T_\gamma(\gamma\simeq1)\equiv T_{\rm FO}$: the orange curve is below the blue one on Fig. 4, bottom panel. Adding the distortions increases even more the rates, and decreases slightly $T_{\rm FO}$ (green curve). One would then expect a reduction of X_n, which would track its equilibrium value longer. While this is true for thermal corrections, adding the distortions disrupts this picture.

Indeed, the detailed balance relation $\overline{\Gamma}_{p\to n} = e^{-\Delta/T}\overline{\Gamma}_{n\to p}$ is not satisfied anymore when including spectral distortions of the neutrinos spectra. Let us parametrize this deviation from detailed balance as

$$\Gamma_{p\to n} = \exp\left(-\frac{\Delta}{T}+\sigma_\nu\right)\Gamma_{n\to p}\,, \tag{30}$$

with $\sigma_\nu \ll 1$. Writing $\overline{\Gamma}$ the Born rates (which satisfy the detailed balance equation), we get

$$\sigma_\nu = \frac{\Delta\Gamma_{p\to n}}{\overline{\Gamma}_{p\to n}} - \frac{\Delta\Gamma_{n\to p}}{\overline{\Gamma}_{n\to p}}\,, \tag{31}$$

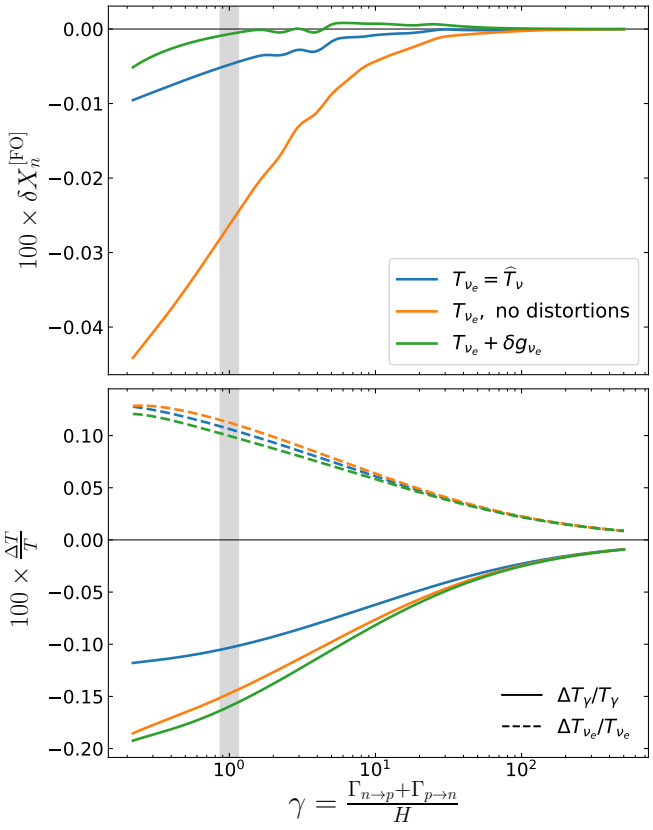

FIG. 4. Neutron fraction (top) and temperatures (bottom) variations at freeze-out, in the different implementations of neutrino-induced corrections.

leading to a change in the equilibrium neutron abundance

$$\delta X_n^{\rm (eq)} = (1-X_n)\sigma_\nu \tag{32}$$

since $X_n/(1-X_n) = n_n/n_p$ and $(n_n/n_p)_{\rm eq} = \Gamma_{p\to n}/\Gamma_{n\to p}$. Corrections to the Born rates are shown on Fig. 5. Equations (30) and thus (32) are not absolutely valid for $\gamma\simeq1$ because deviations from detailed balance start before, but we can nonetheless estimate from this plot $\sigma_\nu(\gamma\simeq1)\simeq0.0008$. With $X_n(\gamma\simeq1)\simeq0.2$, we find from Eq. (32) an *increase* in the neutron fraction at

freeze-out

$$\delta X_n^{[\mathrm{FO}],\delta g_{\nu_e}} \lesssim 0.06\,\%\,, \tag{33}$$

associated to the shift from the orange curve to the green curve on Fig. 4, top panel. This is overestimated because at $\gamma = 1$, the neutron-to-proton ratio has already deviated from nuclear statistical equilibrium. If we consider instead that the shift in $\delta X_n^{[\mathrm{FO}]}$ is due to σ_ν at higher temperatures (namely for $\gamma \sim 3$), we find back the observed shift $\delta X_n^{[\mathrm{FO}],\delta g_{\nu_e}} = 0.03\,\%$.

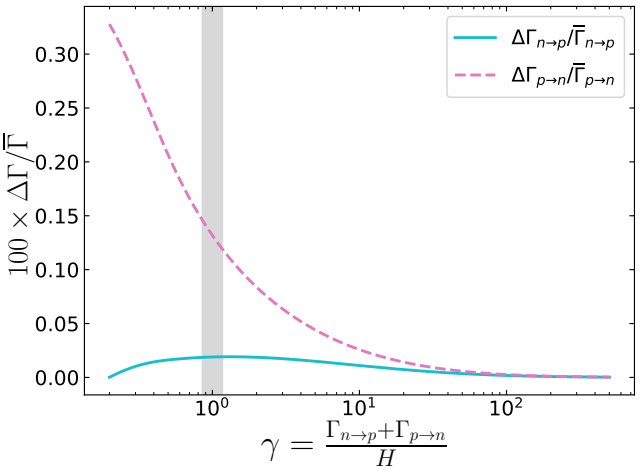

FIG. 5. Relative corrections to $n \leftrightarrow p$ weak rates, with $\Delta\Gamma_{n\leftrightarrow p}$ defined in Eq. (27). To ensure detailed balance requirements, we enforced $T_{\nu_e} = T_\gamma$.

2. *Clock effect*

The *clock effect* is due to the higher radiation energy density for a given plasma temperature, reducing the time necessary to go from T_{FO} to T_{Nuc}. This leads to less neutron beta decay, so a higher $X_n(T_{\mathrm{Nuc}})$ and consequently a higher Y_{P}. To estimate this contribution, we will make several assumptions, justified by observing Fig. 3. Since $t_{\mathrm{Nuc}} \sim 245\,\mathrm{s} \gg t_{\mathrm{FO}}$, the freeze-out modification discussed previously will only result in a very little change in duration: we indeed find numerically $\Delta t_{\mathrm{FO}} \simeq 0.002$ s. We also checked that T_{Nuc} is almost not modified ($\delta T_{\mathrm{Nuc}} \simeq -0.01$ %), which is expected since the onset of nucleosynthesis is essentially determined by T_γ only. Therefore, the clock effect is mainly described by the change of duration between $T_{\mathrm{FO}}^{(0)}$ and $T_{\mathrm{Nuc}} \simeq T_{\mathrm{Nuc}}^{(0)}$.

An additional assumption is made by observing the time scale on Fig. 3: most of neutron beta decay takes place when neutrinos have decoupled and electrons and positrons have annihilated. We will thus consider that between the freeze-out and the beginning of nucleosynthesis, neutrinos are decoupled and $N_{\mathrm{eff}} \simeq N_{\mathrm{eff}}^{\mathrm{fin}}$ is constant.

Therefore, we can write $H \propto 1/2t$ (radiation era). Using Friedmann equation $H^2 \propto \rho$, we get

$$\frac{\Delta t_{\mathrm{Nuc}}}{t_{\mathrm{Nuc}}^{(0)}} = -\frac{1}{2}\,\frac{\Delta\rho}{\rho^{(0)}}\bigg|_{T_\gamma = T_{\mathrm{Nuc}}} = -\frac{1}{2}\,\frac{\Delta\rho_\nu}{\rho_\nu^{(0)}}\bigg|_{T_{\mathrm{Nuc}}} \times \frac{\rho_\nu^{(0)}}{\rho^{(0)}}\,. \tag{34}$$

This shift in the neutrino energy density is parametrized by N_{eff}, while the ratio of instantaneously decoupled energy densities is, at T_{Nuc}, $\rho_\nu^{(0)}/\rho^{(0)} \simeq 0.405$. This gives:

$$\frac{\Delta t_{\mathrm{Nuc}}}{t_{\mathrm{Nuc}}^{(0)}} \simeq -\frac{0.405}{2} \times \frac{\Delta N_{\mathrm{eff}}}{3} \simeq -2.3\times 10^{-3}\,, \tag{35}$$

with $\Delta N_{\mathrm{eff}} = N_{\mathrm{eff}} - 3$ without QED corrections. This estimate is actually in very good agreement with the numerical result

$$\frac{\Delta t_{\mathrm{Nuc}}}{t_{\mathrm{Nuc}}^{(0)}}\bigg|_{\texttt{PRIMAT}} \simeq -2.1\times 10^{-3}\,. \tag{36}$$

Hence the estimate for the clock effect contribution

$$\delta X_n^{[\Delta t]} = -\frac{\Delta t_{\mathrm{Nuc}}}{t_{\mathrm{Nuc}}^{(0)}} \times \frac{t_{\mathrm{Nuc}}^{(0)}}{\tau_n} \simeq 0.064\,\%\,. \tag{37}$$

3. *Helium abundance*

The previous study allows us to estimate the change in ^{4}He abundance. Since most neutrons are converted in ^{4}He, we get in the "complete" case (right T_{ν_e} and spectral distortions included)

$$\delta Y_{\mathrm{P}} = \delta X_n^{[\mathrm{Nuc}]} = \delta X_n^{[\mathrm{FO}]} + \delta X_n^{[\Delta t]} \simeq 0.06\,\%\,, \tag{38}$$

in quite good agreement with the result from Table II. Our value is slightly overestimated, while we would reach an excellent agreement by taking the value $\delta X_n^{[\mathrm{FO}]} = \delta X_n(\gamma \simeq 0.2)$. This can be justified as the criterion $\gamma \sim 1$ for freeze-out is only a rule of thumb, and it was actually pointed out in Ref. [12] that the neutron abundance is only affected by beta decay at $T_\gamma \simeq 3.3\times 10^9$ K, which corresponds to $\gamma \simeq 0.2$.

The different values of δY_{P} depending on the implementations are very well reproduced: since the energy density is always the same, $\delta X_n^{[\Delta t]}$ remains identical, while the varying $\delta X_n^{[\mathrm{FO}]}$ (Fig. 4) controls δY_{P}.

4. *Other abundances*

We now focus on the other light elements produced during BBN, up to ^{7}Be. To understand the individual variations of abundances due to incomplete neutrino decoupling, we separate in Table IV the final abundances of ^{3}He, T and ^{7}Be, ^{7}Li.

	^{3}He/H	T/H	^{7}Be/H	^{7}Li/H
$(i/\mathrm{H})^{(0),\infty}$	$1.06 \cdot 10^{-5}$	$7.84 \cdot 10^{-8}$	$5.36 \cdot 10^{-10}$	$2.79 \cdot 10^{-11}$
$\Delta(i/\mathrm{H})^{\infty}$	$1.3 \cdot 10^{-8}$	$3.2 \cdot 10^{-10}$	$-2.3 \cdot 10^{-12}$	1.1×10^{-13}
$\delta(i/\mathrm{H})^{\infty}$	0.12 %	0.41 %	−0.43 %	0.40 %

TABLE IV. Neutrino-induced corrections to the primordial production of light elements other than ^{4}He and D.

There are two contributions to the change in the final abundance of an element:

$$\begin{aligned}\delta(i/\mathrm{H})^{\infty} &= \delta X_i^{\infty} - \delta X_{\mathrm{H}}^{\infty}\,, \\ &\simeq \delta X_i^{[\Delta t]} + \delta X_n^{[\mathrm{Nuc}]}\,. \end{aligned} \tag{39}$$

The variation of the proton final abundance is directly related to $\delta X_n^{[\mathrm{Nuc}]}$ given in Eq. (26), because an increase of $X_n^{[\mathrm{Nuc}]}$ corresponds to a higher neutron-to-proton ratio and/or less beta decay, so less protons. On the other hand, the variation of X_i^{∞} is entirely encapsulated in $\delta X_i^{[\Delta t]}$, the clock effect contribution (it does not depend on $X_n(T_{\mathrm{Nuc}})$ at first order, since all light elements except ^{4}He are only at the level of traces). Indeed, nucleosynthesis consists in elements being produced/destroyed until the reaction rates, which depend only on T_γ, become too small [39]. Because of incomplete neutrino decoupling, a given value of T_γ is reached sooner and the nuclear reactions have had less time to be efficient. In other words, there is less time to produce or destroy the different elements[5].

We can thus understand the values of Table IV by looking at the evolution of abundances at the end of nucleosynthesis, shown on Fig. 6. All elements except ^{7}Be are mainly destroyed when the temperature has dropped below T_{Nuc}. The very similar evolution of D, T and ^{7}Li explains their close values of δX_i^{∞}: destruction rates are going faster to zero, resulting in a higher final abundance value. For ^{7}Be it is the opposite: it is mainly produced, and the clock effect reduces the quantity possibly formed, hence the negative $\delta X_{^7\mathrm{Be}}^{\infty}$. Moreover its evolution is even sharper than the one of tritium, thus we expect $\left|\delta X_{^7\mathrm{Be}}^{\infty}\right| > \delta X_{\mathrm{T}}^{\infty}$. Finally ^{3}He has much smaller variations, with a little amplitude of abundance reduction from T_{Nuc}. This explains the comparatively small value of $\delta X_{^3\mathrm{He}}^{\infty}$.

To recover the aggregated variations of Table III (for ^{3}He and T ; and ^{7}Be and ^{7}Li), one performs the weighted average of individual variations. Since $(^3\mathrm{He}/\mathrm{H})^{\infty} \gg (\mathrm{T}/\mathrm{H})^{\infty}$, the contribution of ^{3}He dominates ; this argument being immediately transposed to ^{7}Be and ^{7}Li.

[5] This argument does not apply to ^{4}He since it is the most stable light element: for such small variations of the expansion rate, almost all neutrons still end up in ^{4}He, so Y_{P} is only affected by $\delta X_n^{[\mathrm{Nuc}]}$.

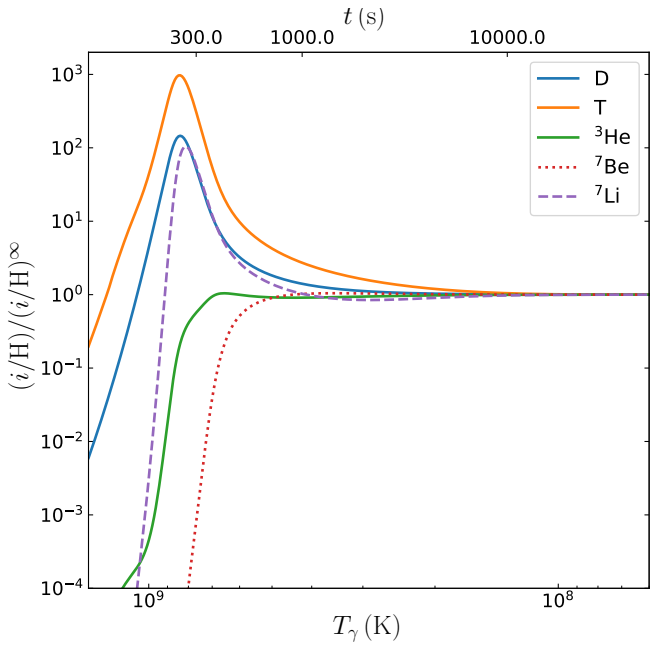

FIG. 6. Evolution of light element abundances computed with `PRIMAT`, including incomplete neutrino decoupling at the Born approximation level. To compare the evolutions for different elements, all abundances are rescaled by their frozen-out value.

C. Precision nucleosynthesis with `PRIMAT`

1. *Full weak rates corrections*

Having thoroughly studied the physics at play by focusing on the Born approximation level, we can now present the results incorporating all weak rates corrections derived in Ref. [12]. These additional contributions (radiative corrections, finite nucleon mass, weak magnetism) cannot in principle be added linearly, due to nonlinear feedback between them. Concerning incomplete neutrino decoupling, this means that we also include radiative corrections inside the spectral distortions part of the rates: we modify Eq. (27) following Eqs. (100) and (103) in Ref. [12].

The results, once again for the three implementations of neutrino-induced corrections, are given in Table V.

Compared to the Born approximation level (Table II), the additional corrections result in higher final abundances, as discussed in Ref. [12]. Starting then from a baseline where all these corrections are included, but not incomplete neutrino decoupling, the shift in abundances due to neutrinos is slightly reduced, by roughly $-0.03\,\%$: for instance $\delta Y_{\mathrm{P}} = +0.02\,\%$ instead of $+0.05\,\%$. The other conclusions of previous sections remain valid: the average temperature implementation is close to the complete one, we explain Y_{P} through $X_n(T_{\mathrm{Nuc}})$ and the clock effect sources the variations of light elements other than ^{4}He.

Since the additional corrections like finite nucleon mass

BBN framework	$Y_{\rm P}$	$\delta Y_{\rm P}$ (%)	D/H $\times 10^5$	δ(D/H) (%)	$\left({}^3{\rm He}+{\rm T}\right)/{\rm H}\times 10^5$	$\left({}^7{\rm Li}+{}^7{\rm Be}\right)/{\rm H}\times 10^{10}$
Inst. decoupling, all corrections	0.24704	0	2.450	0	1.073	5.694
$\widehat{T}_\nu$	0.24709	0.020	2.459	0.36	1.074	5.671
T_{ν_e}, no distortions	0.24699	−0.021	2.458	0.34	1.074	5.669
T_{ν_e}, with distortions	0.24709	0.019	2.459	0.36	1.074	5.671

TABLE V. Light elements abundances, including all weak rates corrections and QED corrections to plasma thermodynamics, for various implementations of neutrino-induced corrections. See Table II for results at the Born approximation level.

contributions only affect the weak rates and not the energy density, we expect that the only difference compared to the picture at the Born level will lie in $\delta X_n^{[\rm FO]}$, while σ_ν and $\delta X_i^{[\Delta t]}$ remain unchanged. This is indeed what we observe on Fig. 7: the neutron fraction at freeze-out reduction due to incomplete neutrino decoupling is enhanced when including all weak rates corrections. Moreover, we read by comparing Figs. 7 and 4

$$\delta X^{[\rm FO]}_{n,\rm All} - \delta X^{[\rm FO]}_{n,\rm Born} \simeq -0.03\,\%\,, \tag{40}$$

which, by injecting this difference in Eqs. (38) and (39), explains the results of Table V.

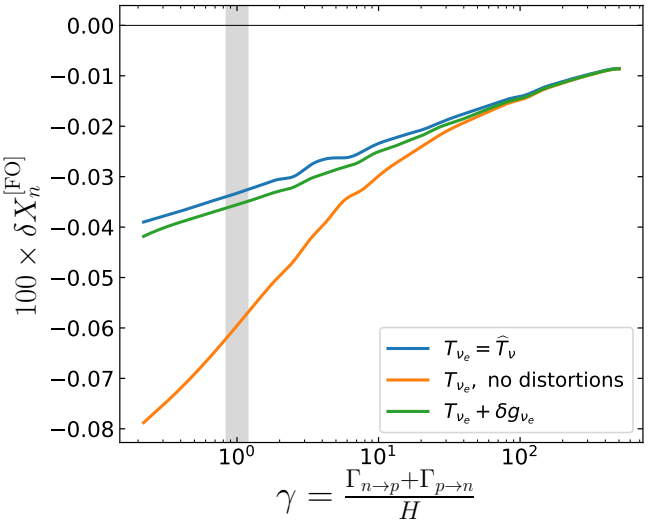

FIG. 7. Neutron fraction around freeze-out, in the different implementations of neutrino-induced corrections. Compared to Fig. 4, all weak rates corrections are included.

2. *What to expect from neutrino oscillations?*

Our findings provide a reasonable guideline for upcoming results including neutrino oscillations. This refinement has been progressively made in neutrino evolution calculations [20, 30], even though some reaction rates (namely neutrino-neutrino scattering) are still approximated. We can anyway forecast the oscillations effect on BBN based on the results of these references. They find that oscillations redistribute the distortions between the different flavors, leaving $N_{\rm eff}$ unchanged, which means that the clock effect contributions will be mostly the same. On the other hand, z_{ν_e} is reduced (and $z_{\nu_{\mu,\tau}}$ increased), with smaller δg_{ν_e} distortions, cf. Fig. 2 in Ref. [20] and Fig. 3 in Ref. [30]. We can thus estimate that, without including the distortions, $\left|\delta X_n^{[\rm FO]}\right|$ will be smaller because of $z_{\nu_e}^{\rm osc.} < z_{\nu_e}^{\rm no\,osc.}$. Put differently, the orange curve on Figs. 4 and 7 will get closer to the blue one. Then, with smaller distortions the deviation from detailed balance will be reduced ($\sigma_\nu^{\rm osc.} < \sigma_\nu^{\rm no\,osc.}$ because $||\delta g_{\nu_e}^{\rm osc.}|| < ||\delta g_{\nu_e}^{\rm no\,osc.}||$), and the compensation observed on Figs. 4 and 7 should mainly subsist, i.e. the green curve will still be close to the blue one.

In other words, results from Refs. [20, 30] indicate that the average temperature implementation should not be modified and would, as in this paper, give remarkably close results to the exact implementation. Therefore we expect that, including neutrino oscillations, their effects should be subdominant compared to our present discussion.

IV. CONCLUSION

In order to assess the consequence of incomplete neutrino decoupling on the production of light elements during BBN, we numerically studied the evolution of neutrinos distribution functions through this epoch. Compared to the instantaneous decoupling case, part of the entropy of $e^\pm$ is transferred to the neutrinos, which results in a decrease of the photon comoving temperature and an increased energy density of neutrinos, parametrized by $N_{\rm eff} \simeq 3.044$ when including QED corrections.

We introduced a parametrization of neutrino distribution functions which conveniently separates the energy density change (via effective temperatures) and the remaining spectral distortions. These quantities, obtained throughout the BBN epoch, have been included in the code `PRIMAT`. The final abundances of light elements, alongside the specific contribution of incomplete neutrino decoupling, are summarized in Table VI. We have been able to scrutinize the physics at play and solve the discrepancy between existing results [20, 21]. The so-called clock effect, due to the increased energy density of neutri-

BBN framework	$Y_{\rm P}$	$\mathrm{D/H}\times10^5$	$\left({}^3\mathrm{He}+\mathrm{T}\right)/\mathrm{H}\times10^5$	$\left({}^7\mathrm{Li}+{}^7\mathrm{Be}\right)/\mathrm{H}\times10^{10}$
Inst. decoupling, all corrections	0.247044	2.45014	1.07276	5.69405
Earlier PRIMAT's approach ($\widehat{T}_\nu$)	0.247093	2.45904	1.07404	5.67079
Incomplete decoupling ($T_{\nu_e}+\delta g_{\nu_e}$)	0.247090	2.45903	1.07404	5.67076
Experimental values [12]	0.2449 ± 0.0040	2.527 ± 0.030	$<1.1\pm0.2$	$1.58^{+0.35}_{-0.28}$

TABLE VI. Light elements abundances from primordial nucleosynthesis, including all corrections derived in Ref. [12]. The erroneous implementation of incomplete neutrino decoupling, through an effective average neutrino temperature and no spectral distortions, matches surprisingly extremely well the actual results. We added a digit compared to Table V to highlight the small difference between the two implementations. We recall for comparison the fiducial abundances obtained in the instantaneous decoupling approximation, and measured values.

nos at a given plasma temperature compared to the fiducial scenario, is responsible for an increase of deuterium and ^{3}He abundances, and a reduction of the quantity of ^{7}Li ; in agreement with Ref. [21].

We found that an approximate implementation, assuming that neutrinos spectra are purely thermally distorted ("thermal-equivalent distortions" introduced in Refs. [20, 37, 38]), works remarkably well if setting all neutrino species to the same temperature. This puzzling feature is due to a compensation between a delayed neutron/proton freeze-out – because of higher weak rates – and a deviation from detailed balance – because of spectral distortions –.

Two additional corrections remain to be included to reach a comprehensive treatment of the physics at play. First, finite temperature QED corrections to the rates of reactions governing neutrino decoupling need to be computed, but as small corrections to collision terms which are already a correction compared to the fiducial cosmology, these ought to be completely negligible. Then, the introduction of neutrino oscillations needs on the contrary to use a density matrix formalism and is numerically much more challenging. However, we argued in Section III C 2 that their effect on primordial nucleosynthesis should be subdominant, thus not modifying our predictions.

ACKNOWLEDGMENTS

JF acknowledges financial support through the graduate program of the École Normale Supérieure. CP and JF thank Cristina Volpe for numerous discussions on neutrino physics.

[1] Y. I. Izotov, T. X. Thuan, and N. G. Guseva, MNRAS **445**, 778 (2014), arXiv:1408.6953.
[2] E. Aver, K. A. Olive, and E. D. Skillman, JCAP **2015**, 011 (2015).
[3] R. J. Cooke, M. Pettini, R. A. Jorgenson, M. T. Murphy, and C. C. Steidel, Astrophys. J. **781**, 31 (2014), arXiv:1308.3240.
[4] R. J. Cooke, M. Pettini, K. M. Nollett, and R. Jorgenson, Astrophys. J. **830**, 148 (2016), arXiv:1607.03900.
[5] R. J. Cooke, M. Pettini, and C. C. Steidel, Astrophys. J. **855**, 102 (2018), arXiv:1710.11129.
[6] N. Aghanim *et al.* (Planck), (2018), arXiv:1807.06209 [astro-ph.CO].
[7] D. A. Dicus, E. W. Kolb, A. M. Gleeson, E. C. G. Sudarshan, V. L. Teplitz, and M. S. Turner, Phys. Rev. **D26**, 2694 (1982).
[8] R. E. Lopez, M. S. Turner, and G. Gyuk, Phys. Rev. **D56**, 3191 (1997), arXiv:astro-ph/9703065 [astro-ph].
[9] R. E. Lopez and M. S. Turner, Phys. Rev. **D59**, 103502 (1999), astro-ph/9807279.
[10] L. S. Brown and R. Sawyer, Physical Review D **63**, 083503 (2001).
[11] P. D. Serpico, S. Esposito, F. Iocco, G. Mangano, G. Miele, and O. Pisanti, JCAP **0412**, 010 (2004), arXiv:astro-ph/0408076 [astro-ph].
[12] C. Pitrou, A. Coc, J.-P. Uzan, and E. Vangioni, Physics Reports **04**, 005 (2018), arXiv:1801.08023.
[13] O. Pisanti, A. Cirillo, S. Esposito, F. Iocco, G. Mangano, G. Miele, and P. Serpico, Computer Physics Communications **178**, 956 (2008).
[14] R. Consiglio, P. de Salas, G. Mangano, G. Miele, S. Pastor, and O. Pisanti, Computer Physics Communications **233**, 237 (2018).
[15] A. Arbey, Computer Physics Communications **183**, 1822 (2012).
[16] A. Arbey, J. Auffinger, K. Hickerson, and E. Jenssen, Computer Physics Communications , 106982 (2019).
[17] C. Pitrou and M. Pospelov, (2019), arXiv:1904.07795 [astro-ph.CO].
[18] A. D. Dolgov, S. H. Hansen, and D. V. Semikoz, Nuclear Physics B **503**, 426 (1997), arXiv:hep-ph/9703315 [hep-ph].
[19] G. Mangano, G. Miele, S. Pastor, and M. Peloso, Physics Letters B **534**, 8 (2002), astro-ph/0111408.
[20] G. Mangano, G. Miele, S. Pastor, T. Pinto, O. Pisanti, and P. D. Serpico, Nuclear Physics B **729**, 221 (2005).
[21] E. Grohs, G. M. Fuller, C. T. Kishimoto, M. W. Paris, and A. Vlasenko, Phys. Rev. D **93**, 083522 (2016).
[22] S. Hannestad and J. Madsen, Phys. Rev. D **52**, 1764 (1995), astro-ph/9506015.

[23] S. Esposito, G. Miele, S. Pastor, M. Peloso, and O. Pisanti, Nuclear Physics B **590**, 539 (2000), astro-ph/0005573.
[24] L. C. Thomas, T. Dezen, E. B. Grohs, and C. T. Kishimoto, arXiv e-prints , arXiv:1910.14050 (2019), arXiv:1910.14050 [hep-ph].
[25] A. F. Heckler, Phys. Rev. D **49**, 611 (1994).
[26] N. Fornengo, C. W. Kim, and J. Song, Phys. Rev. D **56**, 5123 (1997), hep-ph/9702324.
[27] J. J. Bennett, G. Buldgen, M. Drewes, and Y. Y. Y. Wong, arXiv e-prints , arXiv:1911.04504 (2019), arXiv:1911.04504 [hep-ph].
[28] G. Sigl and G. Raffelt, Nuclear Physics B **406**, 423 (1993).
[29] C. Volpe, Int. J. Mod. Phys. **E24**, 1541009 (2015), arXiv:1506.06222 [astro-ph.SR].
[30] P. F. de Salas and S. Pastor, JCAP **2016**, 051 (2016).
[31] A. D. Dolgov, S. H. Hansen, and D. V. Semikoz, Nuclear Physics B **543**, 269 (1999), hep-ph/9805467.
[32] E. Grohs and G. M. Fuller, Nuclear Physics B **923**, 222 (2017).
[33] M. Lucca, N. Schneberg, D. C. Hooper, J. Lesgourgues, and J. Chluba, (2019), arXiv:1910.04619 [astro-ph.CO].
[34] P. Peter and J.-P. Uzan, *Primordial Cosmology*, Oxford Graduate Texts (Oxford University Press, 2013).
[35] J. Lesgourgues, G. Mangano, G. Miele, and S. Pastor, *Neutrino Cosmology* (Cambridge University Press, 2013).
[36] J. Bernstein, L. S. Brown, and G. Feinberg, Rev. Mod. Phys. **61**, 25 (1989).
[37] S. Dodelson and M. S. Turner, Phys. Rev. D **46**, 3372 (1992).
[38] B. D. Fields, S. Dodelson, and M. S. Turner, Phys. Rev. D **47**, 4309 (1993), astro-ph/9210007.
[39] M. S. Smith, L. H. Kawano, and R. A. Malaney, Astrophys. J. Suppl. **85**, 219 (1993).
[40] D. V. Semikoz and I. I. Tkachev, Phys. Rev. D **55**, 489 (1997), hep-ph/9507306.

Appendix A: Neutrino transport equations

Neutrino evolution is computed by simultaneously solving a total of nine equations. The first eight correspond to the rewriting of Boltzmann equations (10) for $i = 0, \ldots, 4$ and $\alpha = e, \mu$. The collision integrals appearing on the right-hand side are reduced to two-dimensional integrals following the method outlined in Refs. [18, 40], and read

$$
\begin{aligned}
C_{\nu_e}(x, y_1) =& \frac{m_e^5 G_F^2}{2\pi^3 y_1 x^5} \int \mathrm{d}y_2\, y_2\, \mathrm{d}y_3\, y_3\, \mathrm{d}y_4\, y_4\, \delta(E_1 + E_2 - E_3 - E_4) \\
&\times \Big\{ F[f_{\nu_e}^{(1)}, f_{\nu_e}^{(2)}, f_{\nu_e}^{(3)}, f_{\nu_e}^{(4)}]\, (6d_1 - 4d_2(1,4) - 4d_2(2,3) + 2d_2(1,2) + 2d_2(3,4) + 6d_3) \\
&+ F[f_{\nu_e}^{(1)}, f_{\nu_e}^{(2)}, f_{\nu_\mu}^{(3)}, f_{\nu_\mu}^{(4)}]\, (4d_1 - 2d_2(1,4) - 2d_2(2,3) + 2d_2(1,2) + 2d_2(3,4) + 4d_3) \\
&+ F[f_{\nu_e}^{(1)}, f_{\nu_e}^{(2)}, f_{\nu_\mu}^{(3)}, f_{\nu_\mu}^{(4)}]\, (2d_1 - 2d_2(1,4) - 2d_2(2,3) + 2d_3) \\
&+ F[f_{\nu_e}^{(1)}, f_{e}^{(2)}, f_{\nu_e}^{(3)}, f_{e}^{(4)}]\, \big[4(g_L^2 + g_R^2)\, (2d_1 - d_2(1,4) - d_2(2,3) + d_2(1,2) + d_2(3,4) + 2d_3) \\
&\qquad - 8 g_L g_R x^2\, (d_1 - d_2(1,3))\, / E_2 E_4 \big] \\
&+ F[f_{\nu_e}^{(1)}, f_{\nu_e}^{(2)}, f_{e}^{(3)}, f_{e}^{(4)}]\, \big[4 g_R^2\, (d_1 - d_2(1,4) - d_2(2,3) + d_3) + 4 g_L^2\, (d_1 - d_2(2,4) - d_2(1,3) + d_3) \\
&\qquad + 4 g_L g_R x^2\, (d_1 + d_2(1,2))\, / E_3 E_4 \big] \Big\},
\end{aligned}
\tag{A1}
$$

$$
\begin{aligned}
C_{\nu_\mu}(x, y_1) =& \frac{m_e^5 G_F^2}{2\pi^3 y_1 x^5} \int \mathrm{d}y_2\, y_2\, \mathrm{d}y_3\, y_3\, \mathrm{d}y_4\, y_4\, \delta(E_1 + E_2 - E_3 - E_4) \\
&\times \Big\{ F[f_{\nu_\mu}^{(1)}, f_{\nu_\mu}^{(2)}, f_{\nu_\mu}^{(3)}, f_{\nu_\mu}^{(4)}]\, (9d_1 - 6d_2(1,4) - 6d_2(2,3) + 3d_2(1,2) + 3d_2(3,4) + 9d_3) \\
&+ F[f_{\nu_\mu}^{(1)}, f_{\nu_e}^{(2)}, f_{\nu_\mu}^{(3)}, f_{\nu_e}^{(4)}]\, (2d_1 - d_2(1,4) - d_2(2,3) + d_2(1,2) + d_2(3,4) + 2d_3) \\
&+ F[f_{\nu_\mu}^{(1)}, f_{\nu_e}^{(2)}, f_{\nu_\mu}^{(3)}, f_{\nu_e}^{(4)}]\, (d_1 - d_2(1,4) - d_2(2,3) + d_3) \\
&+ F[f_{\nu_\mu}^{(1)}, f_{e}^{(2)}, f_{\nu_\mu}^{(3)}, f_{e}^{(4)}]\, \big[4(\tilde{g}_L^2 + g_R^2)\, (2d_1 - d_2(1,4) - d_2(2,3) + d_2(1,2) + d_2(3,4) + 2d_3) \\
&\qquad - 8 \tilde{g}_L g_R x^2\, (d_1 - d_2(1,3))\, / E_2 E_4 \big] \\
&+ F[f_{\nu_\mu}^{(1)}, f_{\nu_\mu}^{(2)}, f_{e}^{(3)}, f_{e}^{(4)}]\, \big[4 g_R^2\, (d_1 - d_2(1,4) - d_2(2,3) + d_3) + 4 \tilde{g}_L^2\, (d_1 - d_2(2,4) - d_2(1,3) + d_3) \\
&\qquad + 4 \tilde{g}_L g_R x^2\, (d_1 + d_2(1,2))\, / E_3 E_4 \big] \Big\}.
\end{aligned}
\tag{A2}
$$

To standardize the notations, we wrote: $d_1 \equiv D_1$, $d_2(i,j) \equiv D_2(i,j)/E_iE_j$ and $d_3 = D_3/E_1E_2E_3E_4$, and

$$F \equiv f^{(3)}f^{(4)}(1-f^{(1)})(1-f^{(2)}) - f^{(1)}f^{(2)}(1-f^{(3)})(1-f^{(4)})\,,$$

the notation $f_a^{(j)}$ meaning $f_a(y_j)$. The functions D_j are defined in Ref. [18]. The weak interaction couplings are $\tilde{g}_L = \sin^2\theta_W + 1/2$ for ν_e, $g_L = \sin^2\theta_W - 1/2$ for $\nu_{\mu,\tau}$ and $g_R = \sin^2\theta_W$ for all species. This difference between flavors is due to charged-current processes ; its consequences were discussed in Section II C. Finally, some typos were corrected compared to the corresponding Eqs. (9)-(10) in Ref. [18].

The last equation describes the evolution of the plasma temperature (cf. Eq. (15) of Ref. [23]),

$$\frac{dz}{dx} = \frac{\frac{x}{z}J(x/z) - \frac{1}{2\pi^2 z^3}\frac{1}{xH}\int_0^\infty \mathrm{d}y\, y^3\left(C_{\nu_e} + 2C_{\nu_\mu}\right)}{\frac{x^2}{z^2}J(x/z) + Y(x/z) + \frac{2\pi^2}{15}}\,, \tag{A3}$$

where we introduced

$$J(\tau) \equiv \frac{1}{\pi^2}\int_0^\infty \mathrm{d}\omega\,\omega^2 \frac{\exp\left(\sqrt{\omega^2+\tau^2}\right)}{\left[\exp\left(\sqrt{\omega^2+\tau^2}\right)+1\right]^2}\,, \tag{A4}$$

$$Y(\tau) \equiv \frac{1}{\pi^2}\int_0^\infty \mathrm{d}\omega\,\omega^4 \frac{\exp\left(\sqrt{\omega^2+\tau^2}\right)}{\left[\exp\left(\sqrt{\omega^2+\tau^2}\right)+1\right]^2}\,. \tag{A5}$$

This equation is derived by rewriting the continuity equation in terms of comoving variables [23].

QED corrections

QED corrections modify in several points the mechanism presented before. In this paper, we only considered the changes to the thermodynamics of the plasma [25–27], since full corrections to the weak rates remain to be calculated, and would correspond to a higher-order effect. We use in the following the notations of Ref. [19]. Changes in the thermodynamics of the electromagnetic plasma induce a decrease of the total pressure

$$P^{\rm int} = -\alpha\pi T_\gamma^4\left(\frac{2}{3}K\left(\frac{m_e}{T_\gamma}\right) + 2K\left(\frac{m_e}{T_\gamma}\right)^2\right)\,, \tag{A6}$$

in agreement with Eq. (48) of Ref. [12]. Note that we only kept the momentum-independent part of the electron mass-shift derived in Ref. [25], as it is the dominant contribution. This result is also in agreement with the limit $m_e \to 0$ used in Ref. [32]. Using the classical thermodynamics relation $\rho = -P + T\mathrm{d}P/\mathrm{d}T$, one derives the energy density contribution corresponding to QED effects:

$$\rho^{\rm int} = \pi\alpha T_\gamma^4\left(-2K - 6K^2 + \frac{2}{3}\frac{m_e}{T_\gamma}K' + 4\frac{m_e}{T_\gamma}KK'\right) \tag{A7}$$

$$= \pi\alpha T_\gamma^4\left(-\frac{2}{3}(K+J) + 2K(K-2J)\right) \tag{A8}$$

where for instance J stands for $J(m_e/T_\gamma)$.

Eq. (A3) is modified by these extra contributions [19]:

$$\frac{dz}{dx} = \frac{\frac{x}{z}J(x/z) - \frac{1}{2\pi^2 z^3}\frac{1}{xH}\int_0^\infty \mathrm{d}y\, y^3\left[C_\nu\right] + G_1(x/z)}{\frac{x^2}{z^2}J(x/z) + Y(x/z) + \frac{2\pi^2}{15} + G_2(x/z)}\,, \tag{A9}$$

The functions G_1 and G_2 are given in Eqs. (18)-(19) of Ref. [19] and Eqs. (4.13)-(4.14) of Ref. [27]. We found a simpler expression of G_1 that we reproduce here:

$$G_1(\tau) = 2\pi\alpha\left[\frac{K'(\tau)}{3} + \frac{J'(\tau)}{6} + J'(\tau)K(\tau) + J(\tau)K'(\tau)\right] \tag{A10}$$

It presents the advantage not to involve a factor $1/\tau$, numerically challenging for high T_γ. It is actually equivalent to the expression in Refs. [20, 27] through the relation:

$$2K(\tau) - \tau K'(\tau) = J(\tau)\,. \tag{A11}$$